

Non-ideal artificial phase discontinuity in long Josephson 0- κ -junctions

T. Gaber,* E. Goldobin, A. Sterck, R. Kleiner, and D. Koelle
*Physikalisches Institut, Experimentalphysik II, Universität Tübingen,
 Auf der Morgenstelle 14, D-72076 Tübingen, Germany*

M. Siegel and M. Neuhaus
Universität Karlsruhe, Institut für Mikro- und Nanoelektronische Systeme, Hertzstr. 16, D-76187 Karlsruhe, Germany
 (Dated: February 2, 2008)

We investigate the creation of an arbitrary κ -discontinuity of the Josephson phase in a long Nb-AlO_x-Nb Josephson junction (LJJ) using a pair of tiny current injectors, and study the formation of fractional vortices formed at this discontinuity. The current I_{inj} , flowing from one injector to the other, creates a phase discontinuity $\kappa \propto I_{\text{inj}}$. The calibration of injectors is discussed in detail. The small but finite size of injectors leads to some deviations of the properties of such a 0- κ -LJJ from the properties of a LJJ with an ideal κ -discontinuity. These experimentally observed deviations in the dependence of the critical current on I_{inj} and magnetic field can be well reproduced by numerical simulation assuming a finite injector size. The physical origin of these deviations is discussed.

PACS numbers: 74.50.+r, 85.25.Cp 74.20.Rp

Keywords: Long Josephson junction, sine-Gordon, half-integer flux quantum, semifluxon, 0- π -junction

I. INTRODUCTION

It has been shown theoretically and experimentally that by utilizing unconventional superconductors or ferromagnetic barriers one can fabricate so-called Josephson π -junctions^{1,2,3,4,5} (π JJs). While for conventional 0-junctions the first Josephson relation reads $I_s = I_c \sin \mu$, for π -junctions it is $I_s = -I_c \sin \mu = I_c \sin(\mu + \pi)$.

In a 1D long Josephson junction (LJJ) with alternating 0 and π regions vortices carrying half of a magnetic flux quantum Φ_0 (so-called semifluxons⁶) can spontaneously appear at the boundaries between 0 and π regions.^{7,8} Such semifluxons were observed experimentally.^{9,10,11,12,13}

In contrast to an integer Josephson vortex (fluxon), which is a free moving soliton, a semifluxon is like a spin $\frac{1}{2}$ particle — it is pinned at a 0- π boundary, has one of two possible polarities $\pm \frac{1}{2}\Phi_0$ and, the most important, can form the groundstate of the system. Semifluxons are very interesting non-linear objects: they can form a variety of groundstates,^{14,15,16,17,18} may flip,^{9,11,19} rearrange¹⁵ or get depinned^{17,20,21} by a bias current, lead to half-integer zero-field steps^{20,21,22} and have a characteristic eigenfrequency.²³ Huge arrays of fractional flux quanta^{9,15,16,17} were realized and predicted to have a tunable plasmon band structure²⁴ which can be thought of as a plasmonic crystal similar to photonic crystals. Semifluxons are also promising candidates for storage devices in classical or quantum domain. They have a very small effective mass³⁶ and the potential for the observation of macroscopic quantum effects and building qubits.

Recently we have demonstrated that one can also study semifluxons in a conventional Nb-AlO_x-Nb LJJ.²² This is done by creating a discontinuity of the Josephson phase ϕ (the difference between ϕ and μ is explained below) by means of current injectors. Two injectors of width Δw are attached to one of the junction's electrodes at

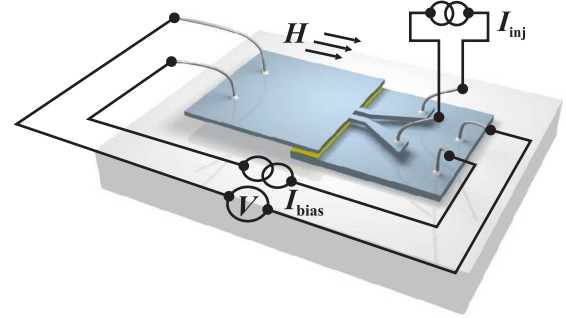


FIG. 1: Sketch of a Josephson junction with a pair of current injectors to create an arbitrary discontinuity of the Josephson phase.

a distance Δx from each other, as shown in Fig. 1. To create an ideal discontinuity, both the injector width Δw and the distance Δx between them must be much smaller than the Josephson penetration depth λ_J . The current I_{inj} , that is passed from one injector to another creates a phase shift $\kappa \propto I_{\text{inj}}$ across the small part $\sim 2\Delta w + \Delta x$ of the top electrode. Since $\kappa \propto I_{\text{inj}}$, the phase shift κ can be tuned to $\kappa = \pi$ by changing I_{inj} . When the discontinuity of the phase is created, the fractional vortex centered at the discontinuity immediately appears to compensate it.

LJJs with such artificially created discontinuities have a number of advantages. First of all, by creating a discontinuity $\kappa \neq \pi$ one can study not only semifluxons, but vortices with any *arbitrary* flux.²⁵ The variable κ can also be used as tuning parameter in some devices, *e.g.*, to tune the plasmon band structure.²⁴ Second, due to low damping in Nb-AlO_x-Nb LJJs one can study the *dynamics* of the fractional vortices. Exponentially low damping at $T \ll T_c$ due to the energy gap also helps to

build qubits with good decoherence figures.

LJJs with double injector structure can also be used for the controllable insertion of an integer fluxon ($\kappa = 2\pi$) into the LJJ,^{26,27} *e.g.*, to set/read out the state of a fluxon or semifluxon based (qu)bit.^{19,28,29} Thus, the structure shown in Fig. 1 can be used in a range of the electronic devices as well as for basic studies involving integer and fractional Josephson vortices.

In experiments, one of the main steps is the calibration of the injectors, *i.e.*, the experimental determination of the ratio κ/I_{inj} . Although a direct theoretical calculation of the ratio κ/I_{inj} is possible in the framework of a 1D model presented below, in practice a different approach is easier and more reliable: one measures the $I_c(I_{\text{inj}})$ dependence and compares it with the $I_c(\kappa)$ dependence obtained theoretically.

The purpose of this paper is to present this calibration method, *i.e.*, study how the $I_c(\kappa)$ and, therefore, the $I_c(I_{\text{inj}})$ dependence should look like for typical experimental parameters. We especially are interested in the effects caused by the finite injector sizes, *i.e.*, when the discontinuity is not an ideal step function.

This paper is organized as follows. In section II we introduce the model of a LJJ with phase discontinuities. In section III we first consider δ -like current injectors that correspond to an ideal step-like discontinuity (or discontinuity *point*) of the Josephson phase and discuss the $I_c(\kappa)$ dependence. In section IV we compare our theory with experimental results. As there are certain misfits between measurements and theoretical predictions, in Sec. V we take the finite size of the injectors into account. Namely, we investigate the effect of the finite injector size on the $I_c(\kappa)$ dependence and on the dependence of I_c on magnetic field H and compare them with experimental results. Section VI concludes this work.

II. THE MODEL

The dynamics of the Josephson phase in a LJJ consisting of 0- and π -parts can be described by the 1D time-dependent perturbed sine-Gordon equation^{6,26,27}

$$\phi_{xx} - \phi_{tt} - \sin \phi = \alpha \phi_t - \gamma(x) - \theta_{xx}(x), \quad (1)$$

where $\phi(x, t)$ is the Josephson phase and subscripts x and t denote the derivatives with respect to coordinate x and time t . In Eq. (1) the spatial coordinate x is normalized to the Josephson penetration depth λ_J and the time t is normalized to the inverse Josephson plasma frequency ω_p^{-1} ; $\alpha = 1/\sqrt{\beta_c}$ is the dimensionless damping parameter; $\gamma = j/j_c$ is the external bias current density normalized to the critical current density of the junction. The function $\theta(x)$ is a step function which is discontinuous at the points where the 0- and π -parts join and constant elsewhere. For example in 0- π -LJJs, $\theta(x)$ can be equal to zero along all 0-parts and to π along all π -parts. For simplicity we assume that there is only one discontinuity point at the center of the junction, $x = 0$.

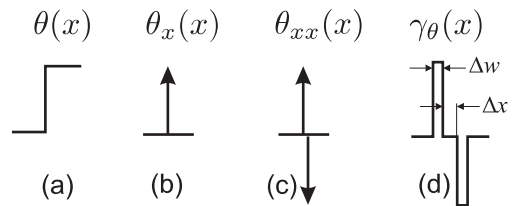


FIG. 2: Functions $\theta(x)$, $\theta_x(x)$, $\theta_{xx}(x)$ and the approximation $\gamma_\theta(x)$ of $\theta_{xx}(x)$ by two rectangular pulses of width Δw and distance Δx .

It is clear from Eq. (1) that the solution $\phi(x)$ is also π -discontinuous at the same points as $\theta(x)$. Therefore, we often call the points where 0- and π -parts join *phase discontinuity points*.

The bias current density $\gamma(x)$ and $\theta_{xx}(x)$ are two additive terms in Eq. (1). This means that if one does not have initially a $\theta_{xx}(x)$ term (like in a conventional LJJ), its effect may be substituted by an additional bias current $\gamma_\theta(x) = \theta_{xx}(x)$. If $\theta(x) = \pi H(x)$ is a step function [Fig. 2(a)], where $H(x)$ is the Heaviside step function, then $\theta_x(x) = \pi\delta(x)$ is a δ -function of strength π [Fig. 2(b)], and $\theta_{xx}(x) = -\pi\delta(x)/x$ [Fig. 2(c)]. Thus the π -discontinuity of the phase corresponds to (or can be substituted by) an additional current with the density $-\pi\delta(x)/x$, *i.e.*, by a *current dipole* of strength π .^{22,26,27} Of course, in experiment one cannot pass infinitely large currents via infinitesimal wires, so the real current profile will be an approximation of $\theta_{xx}(x)$, *e.g.*, like the one shown in Fig. 2(d). Nevertheless, following Ref. 27, we first consider an ideal current dipole (δ -like current dipole) corresponding to an ideal discontinuity.

It is clear, that when we speak in the language of current dipoles we can change the amplitude of the current, *i.e.*, use $-\kappa\delta(x)/x$, which corresponds to a κ -discontinuity of the Josephson phase (instead of a π -discontinuity). Below we consider a LJJ with such an arbitrary κ -discontinuity of the Josephson phase, *i.e.*, $\theta(x) = \kappa H(x)$ in Eq. (1).

Note that other authors^{8,18,30} often use directly the equation written for the *continuous* phase $\mu(x, t)$, which for the case of a κ -discontinuity reads

$$\mu_{xx} - \mu_{tt} \sin(\mu + \theta(x)) = \alpha \mu_t - \gamma(x). \quad (2)$$

Equation (1) and (2) are, actually, equivalent and one can be obtained from the other by substitution $\phi(x, t) = \mu(x, t) + \theta(x)$.⁶ To simulate the system we used the “STKJJ” software,³¹ which implements finite difference algorithms for solving Eq. (2).

III. IDEAL DISCONTINUITY

Using Eq. (1) we first would like to know how the normalized maximum supercurrent

$$i_c = \frac{I_c(\kappa, H)}{I_c(0, 0)}$$

depends on κ . Here i_c can be obtained by varying the normalized supercurrent

$$i = \frac{1}{l} \int_{-l/2}^{l/2} \sin \phi dx$$

with respect to ϕ , which should still be a solution of Eq. (1). The length $l = L/\lambda_J$ is the normalized LJJ length. So far the $i_c(\kappa)$ dependence was calculated only for an annular LJJ.^{27,32} It was predicted and measured²⁶ that this dependence is a Fraunhofer pattern with the first minimum at $\kappa = 2\pi$. This result *does not depend* on the junction length L .

In a junction of linear geometry the situation is different and $i_c(\kappa)$ depends on the normalized length l . Let us first consider extreme cases.

1. $l \gg 1$. In this case one can follow the derivation of Ref. 27 and arrive to the same Fraunhofer pattern (cf. Eq. (10) of Ref. 27)

$$i_c(\kappa) = \left| \frac{\sin(\kappa/2)}{\kappa/2} \right|. \quad (3)$$

On the other hand it is clear, that a κ -discontinuity and a $(\kappa + 2\pi)$ -discontinuity in linear LJJs are physically equivalent, since the phase is defined modulo 2π and there are no topological limits as in annular LJJs. Therefore, the Fraunhofer pattern (3) should be replicated periodically with a period of 2π along the κ -axis, as shown in Fig. 3 (dotted lines). Hence, for a given value of κ one may have more than one i_c , corresponding to different solutions. If one sweeps κ at fixed i , or sweeps i at fixed κ the system may switch from one solution to another by emitting a fluxon which leaves the junction and does not affect the system later. This happens when the bias point crosses one of the dotted lines in Fig. 3. We note that in an annular LJJ a fluxon cannot escape. Therefore transitions as described above (for a linear LJJ) cannot occur, and only the principal Fraunhofer curve Eq. (3) has to be considered. We do not discuss the stability of each solution here, but it is important to note that the topmost branch, indicated by the solid line in Fig. 3, separates all Meissner states from the finite voltage state and can be measured in experiment. Thus, one gets cusp-like minima at $\kappa = \pi + 2\pi n$ (with integer n).

2. $l \ll 1$. In case of a short junction one can neglect the spatial variation of the Josephson phase along the junction and assume that the phase in the left half of the junction is ϕ_0 and in the right half of the junction is $\phi_0 + \kappa$. By varying ϕ_0 we find that the critical current

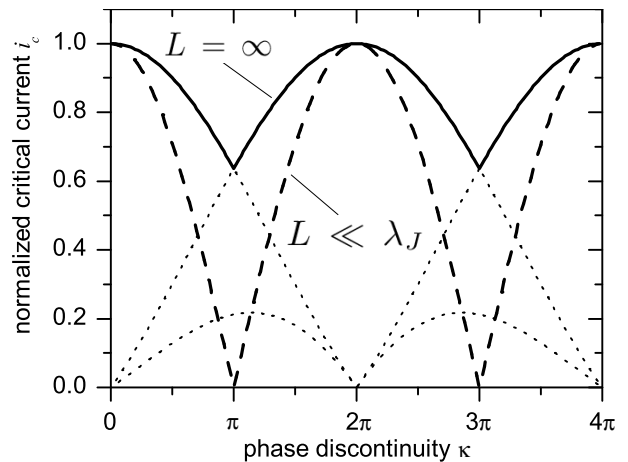


FIG. 3: Dependencies of the normalized critical current i_c on the value of the Josephson phase discontinuity κ . Dotted lines show Fraunhofer patterns (3) shifted by $0, 2\pi, 4\pi$, the corresponding $i_c(\kappa)$ for $L = \infty$ is shown by solid lines. Dashed lines show the dependence (4) for $L \ll \lambda_J$.

depends on κ as

$$i_c(\kappa) = \left| \cos\left(\frac{\kappa}{2}\right) \right|, \quad (4)$$

which is shown in Fig. 3 by the dashed line.

In Fig. 3 one can see that both dependences have a common feature: they have maxima at $\kappa = 2\pi n$ and cusp-like minima (possibly with hysteresis) at $\kappa = \pi + 2\pi n$. The value of i_c at the minima depends on the junction length and varies from 0 for a short junction to $2/\pi$ for an infinitely long one.

3. Intermediate l . In this case the $i_c(\kappa)$ curve lies in between the two curves for $l \ll 1$ and $l \gg 1$, but still has cusp-like minima at $\kappa = \pi(2n + 1)$. The numerically calculated dependence of the minimum critical current $i_c(\pi)$ on junction length will be shown later in Sec. V. Since cusp-like minima in $i_c(\kappa)$ always correspond to a phase discontinuity $\kappa = (2n + 1)\pi$, the calibration process of the injectors is simple. One should measure $I_c(I_{inj})$. Since $\kappa \propto I_{inj}$ the value of I_{inj} at the first cusp-like minimum of the $I_c(I_{inj})$ dependence corresponds to $\kappa \bmod 2\pi = \pi$.

IV. SAMPLES

So far an ideal κ -discontinuity or, to put it in terms of an additional bias current, δ -like current injectors were discussed and the $i_c(\kappa)$ dependence was investigated. As a result we saw that the $i_c(\kappa)$ curve is 2π periodic and has a minimum of the critical current for phase discontinuities $\kappa = (2n + 1)\pi$ independent of the junction length. In order to experimentally investigate artificial 0 - κ -LJJs we used samples that were fabricated at the University of Karlsruhe as well as by Hypres³⁷ and that are based

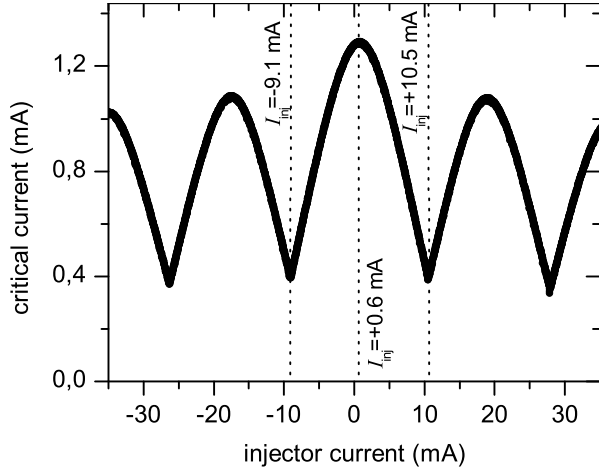


FIG. 4: Experimentally measured $I_c(I_{\text{inj}})$ dependence at $H = 0$ (sample #2).

on conventional Nb-AlO_x-Nb technology. All data presented here have been obtained at $T = 4.2$ K from different samples with parameters summarized in Tab. I. For all samples the junction layout is identical to the one presented in Fig. 1. A photograph can be found in Fig. 3 of Ref. 22 (sample #4 in Tab. I). However, the values of λ_J , the lengths L and the injector sizes are different. For all samples the I - V characteristics (IVC) and the dependences of $I_c(H)$ without injector current were measured to ensure good sample quality and the absence of trapped magnetic flux (not shown).

Figure 4 shows a typical measurement of $I_c(I_{\text{inj}})$ at $H = 0$, obtained from sample #2. One can clearly see the almost periodic modulation of the critical current as a function of I_{inj} which is very similar to the one predicted in Fig. 3. Yet, there is an unexpected decrease of I_c at the side maxima $I_{\text{inj}} \approx \pm 19$ mA. We have also measured the $I_c(H)$ dependence at I_{inj} corresponding to the first minimum in the $I_c(I_{\text{inj}})$ dependence, *i.e.*, the $I_c(H)$ dependence in the 0 - π -state. Such a dependence is expected to have a minimum of I_c at $H = 0$.^{18,33} In Fig. 5 two typical $I_c(H)$ dependences experimentally obtained from different samples are presented. Although we indeed observe a minimum of I_c at $H = 0$,^{5,33} the curves in Fig. 5 are rather asymmetric with respect to $H = 0$:²² the amplitudes of the first maxima are different and the higher order maxima have different, sometimes not very regular, periods.

In the following we show that these deviations can be reproduced in numerical simulations using the model with the finite size of the injectors. The physical origin of these deviations is discussed.

V. NON-IDEAL DISCONTINUITY

To model the finite-sized injectors we used the current injection profile $\gamma_\theta(x)$ shown in Fig. 2(d). Note that

this shape is a rather simple, but decent approximation, corresponding to our system with superconducting injectors and a ground plane. Also, we consider here a 1D model, whereas in the real geometry (see Fig. 1 or Fig. 3 of Ref. 22) the injector current may be distributed in a rather peculiar way across the top electrode.

Equation (1) can be rewritten as

$$\phi_{xx} - \phi_{tt} - \sin \phi = \alpha \phi_t - \gamma - \gamma_\theta(x), \quad (5)$$

where $\gamma_\theta(x)$ approximates $\theta_{xx}(x)$. By introducing a finite injector size the κ -discontinuity is now stretched over a finite distance $\Delta l = 2\Delta w + \Delta x$. In the injector area the dynamics of the Josephson phase and therefore the junction properties are dominated by the injector current distribution.

First, we are interested in the static phase profile in the injector area. If the injectors provide the current density distribution $\gamma_\theta(x)$, the static sine-Gordon equation is

$$\phi_{xx} = \sin \phi - \gamma - \gamma_\theta(x). \quad (6)$$

For the following considerations it is more convenient to separate the amplitude γ_{inj} of the injector current density from the actual injection profile

$$\tilde{\gamma}_\theta(x) = \begin{cases} 1 & , -\frac{\Delta l}{2} < x < -\frac{\Delta x}{2} \\ 0 & , -\frac{\Delta x}{2} < x < +\frac{\Delta x}{2} \\ -1 & , +\frac{\Delta x}{2} < x < +\frac{\Delta l}{2} \end{cases}, \quad (7)$$

so that $\gamma_\theta(x) = \gamma_{\text{inj}} \tilde{\gamma}_\theta(x)$. In the injector region, $\gamma_\theta(x)$ provides the dominating contribution ($|\gamma_{\text{inj}}| \gg 1$) to the rhs. of Eq. (6). If in addition Δx is assumed to be $\ll 1$, Eq. (6) can be simplified to

$$\phi_{xx} = -\gamma_{\text{inj}} \tilde{\gamma}_\theta(x). \quad (8)$$

Double integration of Eq. (8) gives the phase profile $\phi(x)$ in the region of injectors ($-\Delta l/2 < x < +\Delta l/2$) depicted in Fig. 6. The difference of the phase $\phi(\Delta l/2) - \phi(-\Delta l/2)$ is proportional to γ_{inj} and should be equal to κ . Thus we obtain a relation between κ and the amplitude of the injector current density γ_{inj}

$$\kappa = -\gamma_{\text{inj}} \Delta w (\Delta w + \Delta x). \quad (9)$$

Now, let us consider the effect of a finite injector size on the $i_c(\kappa)$ dependence. Fig. 7 shows two sets of numerically calculated $i_c(\kappa)$ curves. In Fig. 7(a) junctions of the same length $L = 2\lambda_J$ but different injector sizes are compared, ranging from $\Delta x = 0, \Delta w = 0$ (ideal discontinuity) to $\Delta w = 0.32, \Delta x = 0.33$. The most prominent difference compared to an ideal discontinuity is a decrease in critical current at the side maxima $i_c(2\pi n)$ ($n \neq 0$). The difference of critical currents $i_c(0) - i_c(2\pi n)$ becomes smaller as the injector size is reduced and approaches zero as injectors become ideal ($\Delta x \rightarrow 0, \Delta w \rightarrow 0$). In addition the minima of the curve shift slightly towards values of $|\kappa| > \pi(2n + 1)$ and $i_{c,\text{min}}$ is slightly reduced when injectors become very large and comparable to the Josephson

chip	j_c [A/cm ²]	λ_J [μ m]	length L [μ m]	norm. length l	injector width [μ m]	Δw	injector distance [μ m]	Δx	N
#1 ^a	≈ 150	≈ 24	30–360	1.25–15	5	0.21	5	0.21	7
#2 ^a	≈ 400	≈ 15	60	4	2	0.13	2	0.13	1
#3 ^a	≈ 400	≈ 15	120	8	5	0.33	5	0.33	1
#4 ^b	≈ 100	≈ 30	60	2	5	0.17	4	0.13	2

^afabricated at the University of Karlsruhe, Germany.

^bfabricated by Hypres, Elmsford, New York, USA.

TABLE I: Sample properties. The quantities l , Δw and Δx are the normalized (with respect to λ_J) LJJ length, injector width and distance between the injectors. N is the number of junctions on the chip, that were measured. The junction width is $5 \mu\text{m}$ for all samples.

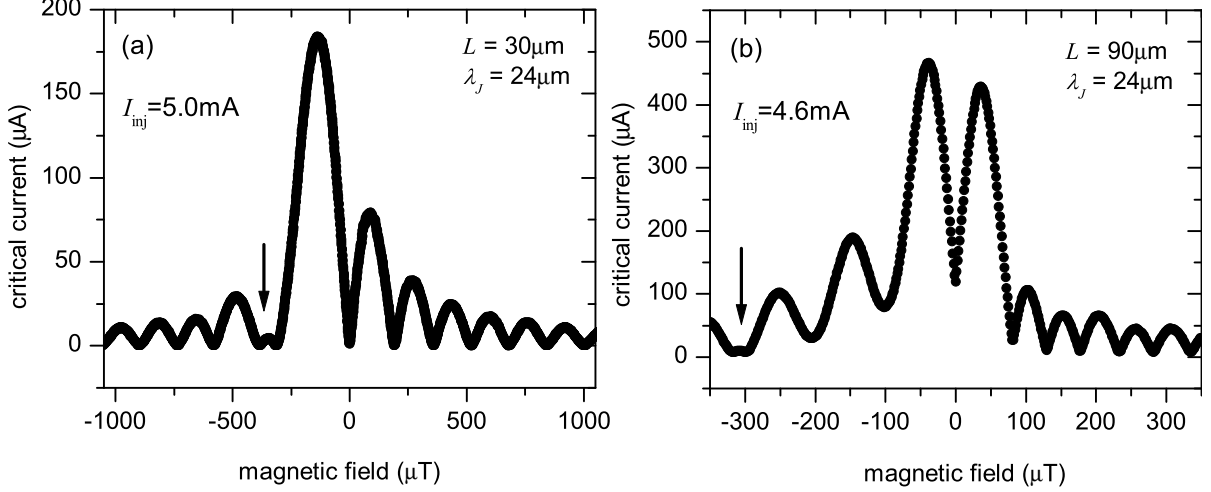


FIG. 5: Measured $I_c(H)$ dependences in the $0-\pi$ -state for two LJJ (chip #1) of length $L = 1.25 \lambda_J$ (a) and $L = 3.75 \lambda_J$ (b). Arrows mark the crossing of the H -axis in negative fields [cf. Fig. 12 (b)].

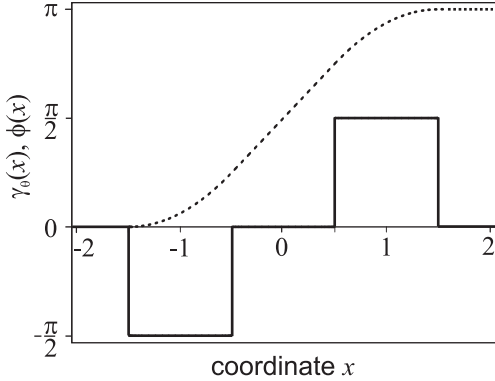


FIG. 6: Spatial dependence of $\gamma_\theta(x)$ (solid line) and $\phi(x)$ (dotted line) in the injector area. $\Delta x = \Delta w = 1$, $\gamma_{\text{inj}} = -\pi/2$ for simplicity. The injector size is intentionally chosen to be huge ($\sim \lambda_J$) to visualize the behavior of the Josephson phase in all regions.

penetration depth. The last effect is rather small and can normally be neglected for typical sizes of injectors. Fig. 7(b) shows the $i_c(\kappa)$ dependence of junctions with the same injectors, but for different LJJ lengths. Again, there is a decrease of $i_c(2n\pi)$ for $n \neq 0$; yet, with increas-

ing junction length L the $i_c(\kappa)$ dependence approaches the curve of an ideal discontinuity (see Fig. 3).

Fig. 8 shows the numerically calculated dependence of the minimum critical current $i_{c,\text{min}}$ at $\kappa \approx \pi$ on LJJ length L , for ideal and non-ideal discontinuities, as well as experimentally obtained results. The numerical calculations for the case of finite injector size were performed with $\Delta w = 0.2$, $\Delta x = 0.21$, comparable to the experimental dimensions of sample series #1. In the simulations the finite injector size has a negligible influence on $i_{c,\text{min}}$. However, for $L < 10 \lambda_J$ the experimentally determined values of $i_{c,\text{min}}$ are systematically *smaller* than theory predicts. Only for very long JJs, $L \geq 10 \lambda_J$, measurements and theory approach the same asymptotic value of $2/\pi$ (semifluxon depinning current^{15,16,34}). It is interesting to note, that the measured values (except for sample #2, that has smaller injectors) show a similar dependence as in theory, yet the experimental data seem to be shifted along the L -axis, towards longer JJs. So far this behavior is not fully understood. However the better agreement between theory and experimental data for sample #2 gives already an indication, that the actual injector size does play an important role and that the 1D model for the injectors could be too simple.

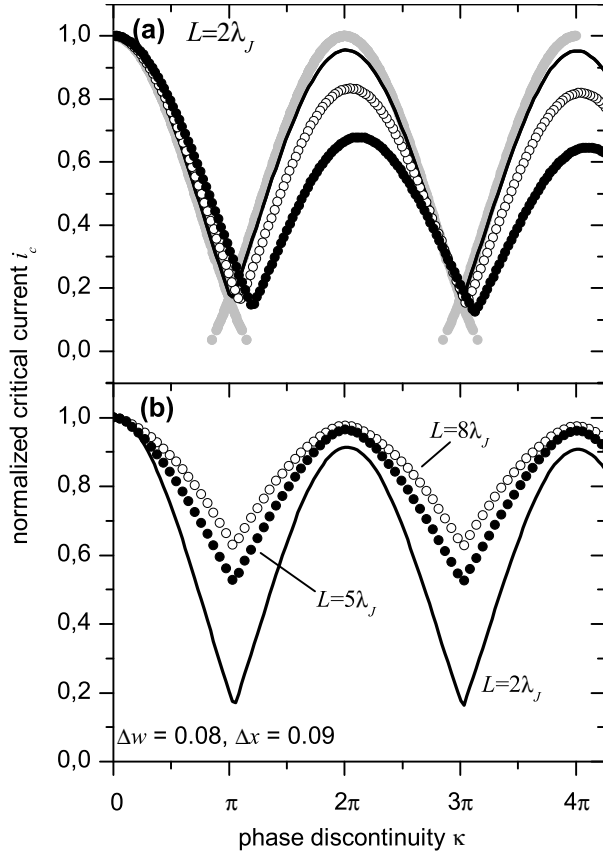


FIG. 7: Normalized critical current i_c vs. the Josephson phase discontinuity κ , numerically calculated for junctions with fixed $L = 2\lambda_J$ and different injectors (a) and junctions with same injectors ($\Delta w = 0.08$, $\Delta x = 0.09$) but different L (b). In (a) the sizes of injectors are $\Delta x = 0$, $\Delta w = 0$ (gray circles), $\Delta w = 0.04$, $\Delta x = 0.05$ (solid line), $\Delta w = 0.16$, $\Delta x = 0.17$ (open circles) and $\Delta w = 0.32$, $\Delta x = 0.33$ (black circles).

Looking at the *maxima* in Fig. 7 again, we conclude that the deviations from the ideal characteristics depend on the relative size of the injector region with respect to the junction length. There is a simple picture to understand this qualitatively. For example, at $\kappa = 2\pi$ the Josephson phase increases by 2π , from $\phi(-\Delta l/2)$ to $\phi(+\Delta l/2)$ in the region between the injectors, so that in this region the net Josephson current across the junction can be neglected (if the increase in ϕ is linear), no matter what bias current is applied, because $\gamma \ll \gamma_{\text{inj}}$. Therefore the junction length L is effectively reduced by the size of the injector region and to a first order approximation the critical current is $i_c(\pm 2\pi) \approx 1 - (\Delta w + \Delta x)/l$. Note, that the effective injector region, that has a net Josephson current equal to zero, is only $\Delta x + \Delta w$ rather than $\Delta x + 2\Delta w$, due to the parabolic shape of ϕ inside the injector electrodes (cf. Fig. 6). In Fig. 9 we plot $\Delta i_c = 1 - i_c(2\pi)$ vs. $(\Delta w + \Delta x)/l$ obtained experimentally and numerically for junctions with different injector sizes and of different LJJ lengths l . One can notice, that

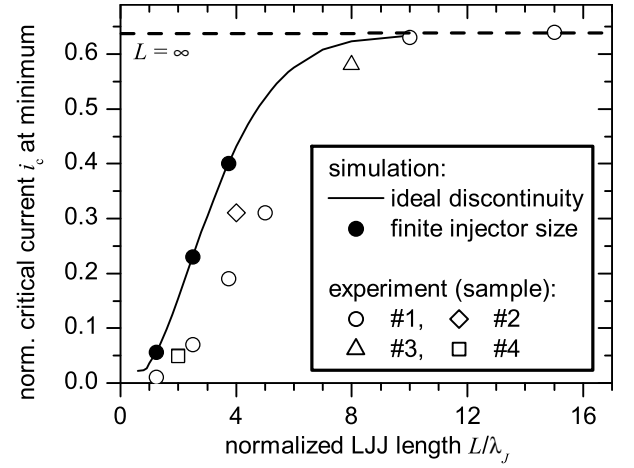


FIG. 8: Minimum normalized critical current i_c vs. junction length numerically calculated for an ideal discontinuity (solid line) and non-ideal injectors with $\Delta x = 0.21$, $\Delta w = 0.2$ (solid circles). Open symbols correspond to measurements of the samples summarized in Tab. I.

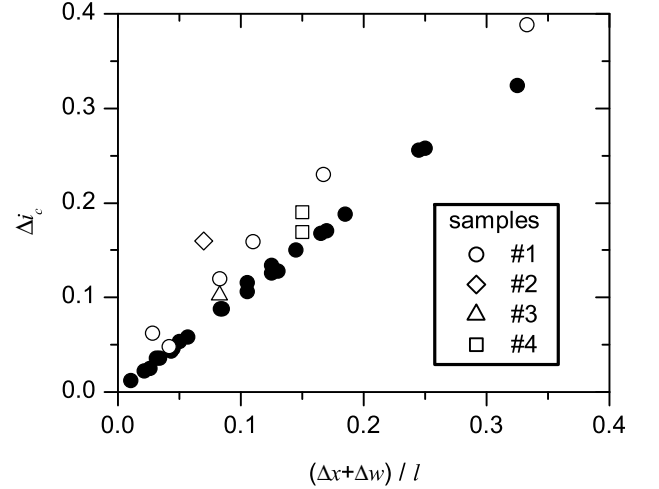


FIG. 9: Numerically calculated (filled circles) and measured (open symbols) reduction of normalized critical current $\Delta i_c = 1 - i_c(2\pi)$ for different junction lengths and injector sizes.

the experimental data are in a good agreement with numerical calculations, yet the measured drop in critical current is always slightly larger than the theory predicts. By confining even larger phase jumps ($\kappa = 4\pi, 6\pi, \dots$) into the area of injectors, the critical current of the junction slowly decreases further (see Fig. 7). Yet, the relative change $i_c(2\pi n) - i_c(2\pi(n+1))$, $n > 0$ is much smaller than $\Delta i_c = 1 - i_c(\pm 2\pi)$ and depends on the details of the phase bending inside the injector area. This, however is a higher order effect which is not addressed in this paper, because in experiments one always wants to have $\Delta x, \Delta w \ll 1$.

Now let us concentrate on the $0-\pi$ -state [I_{inj} corresponding to a minimum in $I_c(I_{\text{inj}})$] and consider the

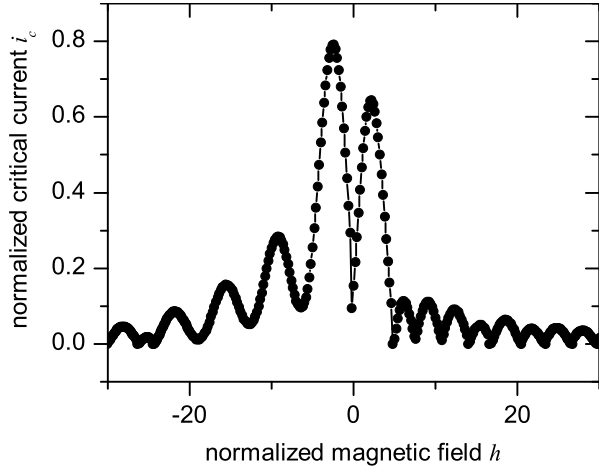


FIG. 10: Numerically calculated $i_c(h)$ dependence of a LJJ ($L = 2\lambda_J$) in the 0- π -state. Injector size is $\Delta w = 0.16$ and $\Delta x = 0.13$.

$i_c(h)$ dependence, where $h = 2H/H_{c1}$ and $H_{c1} = \Phi_0/(2\pi\mu_0\lambda_L\lambda_J)$ is the first critical field for a LJJ with thick electrodes. In Fig. 10 we show the numerically calculated $i_c(h)$ dependence of an artificial 0- π -LJJ with finite injectors. Parameters are chosen to be comparable with experimental dimensions²² (cf. sample #4). As has already been mentioned in Ref. 22, simulated results reproduce all features of the experimentally measured $I_c(H)$ dependence rather well [see Fig. 5(b) or Fig. 5 in Ref. 22]. Although the curve shown in Fig. 10 has the characteristic minimum of the critical current in zero magnetic field, it is rather asymmetric. The maximum critical currents of the side lobes are different and the periodicities of the outer oscillations for negative and positive field differ. Yet, with decreasing injector size this asymmetry disappears as can be seen in Fig. 11.

To understand the reason for this asymmetries, we, for the moment, consider a relatively short JJ ($L \lesssim \lambda_J$) and find the expression for $i_c(h)$ for injectors having a normalized size Δw and distance Δx between them. The Josephson phase is assumed to be linear outside the injector area, *i.e.*,

$$\phi_{out}(x) = \begin{cases} \phi_0 + h \left(x + \frac{\Delta l}{2} \right) & , \quad -\frac{l}{2} < x < -\frac{\Delta l}{2} \\ \phi_0 + \kappa + h \left(x - \frac{\Delta l}{2} \right) & , \quad +\frac{\Delta l}{2} < x < +\frac{l}{2} \end{cases} \quad (10)$$

Inside the injector region the phase changes from ϕ_0 to $\phi_0 + \kappa$ over the distance $\Delta l = 2\Delta w + \Delta x$, but its particular profile will be discussed later.

The total supercurrent carried by the LJJ outside the injector area is calculated by integrating $\sin \phi_{out}(x)$ over the junction length excluding the injector region. By varying ϕ_0 to maximize i_c we find that the maximum i_c is reached at

$$\phi_0 = \frac{\pi}{2} - \frac{\kappa}{2}, \quad (11)$$

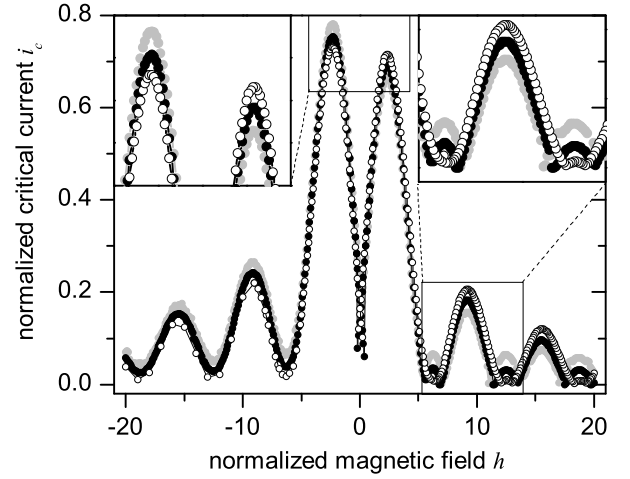


FIG. 11: Numerically calculated $i_c(h)$ dependence of a LJJ ($L = 2\lambda_J$) in the 0- π -state. Injectors have a width/distance of $\Delta w = 0.01/\Delta x = 0.011$ (open circles), $\Delta w = 0.04/\Delta x = 0.05$ (black filled circles) and $\Delta w = 0.08/\Delta x = 0.09$ (gray filled circles).

and is given by

$$i_c(h) = \frac{4}{hl} \cos \frac{\kappa + h(l - \Delta l)}{2} \sin \frac{h(l - \Delta l)}{2}. \quad (12)$$

The dependence (12) is an odd function of h , *i.e.*, it is anti-symmetric with respect to the origin $h = 0$. We note that in experiment one always measures the absolute value $|i_c(h)|$, which is a *symmetric* (even) function with respect to the origin $h = 0$, and has a minimum at $h = 0$.

Now let us calculate the supercurrent carried by the region of injectors. The phase $\phi(x)$ changes from ϕ_0 to $\phi_0 + \kappa$ as shown in Fig. 6, *i.e.*, it has two parabolic parts corresponding to two injectors and a linear part corresponding to the spacing between injectors. To calculate the supercurrent $i_{s, \text{inj}}$ carried by the injector region, we again integrate

$$i_{s, \text{inj}} = \frac{1}{l} \int_{-\Delta l/2}^{+\Delta l/2} \sin \phi(x) dx. \quad (13)$$

Since some parts of $\phi(x)$ are parabolic, we will end up with Fresnel integrals which will only add additional complications. We thus change the phase profile a little bit to simplify integration, taking into account that the injector current profile shown in Fig. 2 is only a simple approximation. Considering that in our original model $\phi(x)$ changes parabolically, *i.e.*, slowly, and that for superconducting injectors most of the current flows close to the inner edge of the injector, we adopt a very simple injector phase profile

$$\phi(x) = \phi_0 + \kappa \left(\frac{x}{\Delta x + \Delta w} + \frac{1}{2} \right), \quad -\frac{\Delta x + \Delta w}{2} < x < +\frac{\Delta x + \Delta w}{2}, \quad (14)$$

i.e., the phase changes linearly from ϕ_0 to $\phi_0 + \kappa$ only in the space between the injector centers. By effectively shortening the injector area, the still unattended outer halves of the injectors are simply added to the part of the LJJ without injectors, *i.e.*, we substitute $\Delta \tilde{l} = \Delta w + \Delta x$ for Δl in Eqs. (10), (12) and (13). Thus, the supercurrent (13) carried by the injector region calculated for optimum ϕ_0 (11) is

$$i_{s,\text{inj}} = (\Delta x + \Delta w) \frac{2}{\kappa l} \sin \frac{\kappa}{2}. \quad (15)$$

Note, that $i_{s,\text{inj}}$ does not depend on magnetic field, because we did not take the penetration of magnetic field into the injector region into account.

The resulting normalized maximum supercurrent *vs.* field dependence which one measures in experiment is given by

$$i_s(h) = |i_c(h) + i_{s,\text{inj}}|, \quad (16)$$

i.e., the anti-symmetric $i_c(h)$ dependence from Eq. (12) is first shifted along the i -axis by $i_{s,\text{inj}}$ and then the absolute value is calculated, [see Fig. 12 (a)]. As a result one gets asymmetric maxima for $h > 0$ and $h < 0$. Moreover, the side oscillations of $i_c(h) + i_{s,\text{inj}}$ due to the shift may not intersect the h -axis anymore for $h < 0$, but do intersect it for $h > 0$, resulting in very different patterns of the side maxima for the $i_s(h)$ dependence, [see Fig. 12(a)].

Before we proceed with a comparison of experiment with our analytical results, we would like to note another effect which may become noticeable in not very long junctions with rather large injectors. Namely, the phase jump κ which, up to now, was supposed to be only due to the injector current $\kappa = \kappa_{\text{inj}}$, can also have a contribution from the magnetic field penetrating the injector area. We write $\kappa = \kappa_{\text{inj}} + h(\Delta x + \Delta w)$ and use the so-defined κ in Eq. (15) and (16). Then, the contribution of the injector area to the supercurrent, *i.e.*, the above mentioned shift, becomes field dependent. This means that side oscillations of $i_c(h) + i_{s,\text{inj}}$ which did not cross the ($i_s = 0$)-axis for lower fields, may do so for larger fields, as is shown in Fig. 12(b). The larger the ratio $(\Delta x + \Delta w)/l$ the more noticeable this effect will be. Fig. 5 shows experimentally obtained $I_c(H)$ -dependences of two LJJ of different length in the $0-\pi$ -state. As one can see clearly, these measurements are in good agreement with the above calculations. In particular, one can notice that the shorter the JJ is, the more pronounced is the asymmetry in $i_c(h)$.

It is interesting to note, that with the simple short junction model presented above, almost all features of

the measured $I_c(H)$ dependence can be explained and effectively pinpointed to the supercurrent inside the injector area.

VI. CONCLUSIONS

A pair of tiny current injectors can be used to create an arbitrary phase jump of the Josephson phase and to study arbitrary fractional vortices pinned at it. An important step, which one should make following this approach, is to calibrate the injectors, *i.e.*, to measure the $I_c(I_{\text{inj}})$ dependence. Here we calculated how $I_c(I_{\text{inj}})$ should look like in the $0-\kappa$ -LJJ of length L with an ideal discontinuity. We discuss the effect of finite injector size on the $I_c(I_{\text{inj}})$ and $I_c(H)$ dependence and find rather good agreement between our model and experimental data. The consequences of finite sized injectors compared to an ideal discontinuity can be summarized as follows:

(I) The $i_c(\kappa)$ dependence is not perfectly 2π periodic but exhibits a decrease in $i_c(\pm 2n\pi) < 1$, $n \neq 0$. The drop of i_c at $\kappa = \pm 2\pi$ can roughly be estimated as $1 - i_c(\pm 2\pi) \approx (\Delta w + \Delta x)/l$ and is associated with the exclusion of injector area that carries no net supercurrent.

(II) The $i_c(h)$ characteristic for $\kappa = \pi$ is asymmetric with respect to magnetic field. This asymmetry is caused by the Josephson currents flowing in the area between the injectors. These Josephson currents shift the $i_c(h)$ curve by $i_{s,\text{inj}}$ [cf. Eq. (15)] and become weakly field dependent for $\Delta l \lesssim l$. As in experiment only $i_s(h) = |i_c(h) + i_{s,\text{inj}}|$ can be measured, yet $i_c(h)$ is an odd function of h , parts of the $i_c(h)$ curve get reflected at the h -axis, resulting in a field dependent and asymmetric pattern of the higher order maxima. The difference in normalized critical current between the main maxima is $\approx \pm \frac{4}{\pi}(\Delta x + \Delta w)/l$ with respect to ideal injectors.

In general, it is desirable to make the injector region as small as possible, to avoid the discussed finite size effects. However, for cases where this is not possible, our results allow one to interpret the experimental data properly and optimize the design of such LJJs.

Acknowledgments

This work was supported by the Deutsche Forschungsgemeinschaft (project GO-1106/1) and by the ESF program "PiShift".

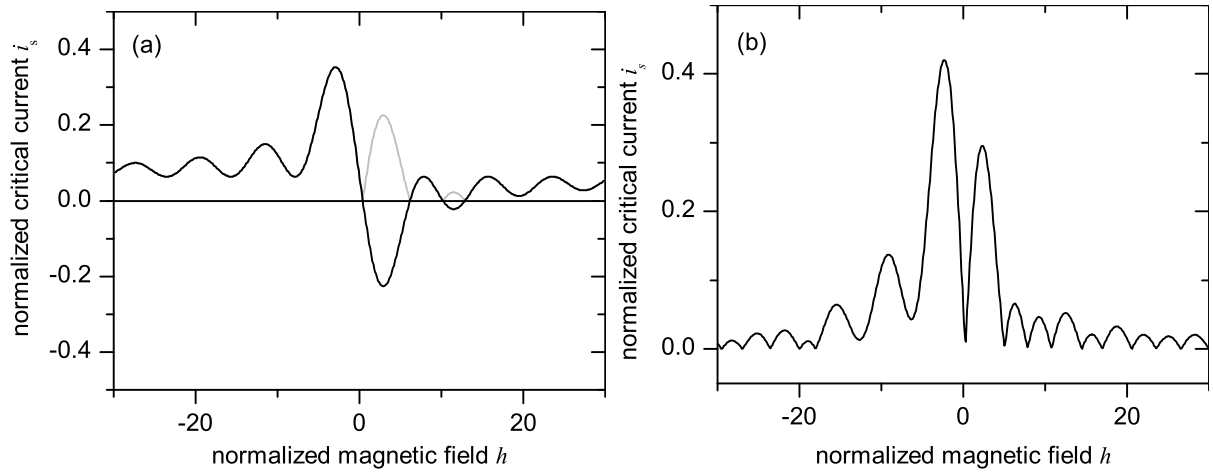


FIG. 12: (a): Calculated dependence of $i_s(h)$ (black line) and $|i_s(h)|$ (gray line). (b): Calculated dependence of $|i_s(h)|$ in case magnetic field is penetrating the injector area. Parameters are $l = 2$, $\kappa = \pi$ and $\Delta x = \Delta w = 0.2$.

-
- * Electronic address: gaber@uni-tuebingen.de
- ¹ L. N. Bulaevskii, V. V. Kuzii, and A. A. Sobyanin, JETP Lett. **25**, 290 (1977), [Pis'ma Zh. Eksp. Teor. Fiz. **25**, 314 (1977)].
 - ² T. Kontos, M. Aprili, J. Lesueur, F. Genêt, B. Stephanidis, and R. Boursier, Phys. Rev. Lett. **89**, 137007 (2002).
 - ³ V. V. Ryazanov, V. A. Oboznov, A. Y. Rusanov, A. V. Veretennikov, A. A. Golubov, and J. Aarts, Phys. Rev. Lett. **86**, 2427 (2001).
 - ⁴ F. Lombardi, F. Tafuri, F. Ricci, F. Miletto Granozio, A. Barone, G. Testa, E. Sarnelli, J. R. Kirtley, and C. C. Tsuei, Phys. Rev. Lett. **89**, 207001 (2002).
 - ⁵ D. J. V. Harlingen, Rev. Mod. Phys. **67**, 515 (1995).
 - ⁶ E. Goldobin, D. Koelle, and R. Kleiner, Phys. Rev. B **66**, 100508(R) (2002).
 - ⁷ L. N. Bulaevskii, V. V. Kuzii, and A. A. Sobyanin, Solid Stat. Comm. **25**, 1053 (1978).
 - ⁸ J. H. Xu, J. H. Miller, and C. S. Ting, Phys. Rev. B **51**, 11958 (1995).
 - ⁹ H. Hilgenkamp, Ariando, H.-J. H. Smilde, D. H. A. Blank, G. Rijnders, H. Rogalla, J. R. Kirtley, and C. C. Tsuei, Nature (London) **422**, 50 (2003).
 - ¹⁰ J. R. Kirtley, C. C. Tsuei, M. Rupp, J. Z. Sun, L. S. Yu-Jahnes, A. Gupta, M. B. Ketchen, K. A. Moler, and M. Bhushan, Phys. Rev. Lett. **76**, 1336 (1996).
 - ¹¹ J. R. Kirtley, C. C. Tsuei, and K. A. Moler, Science **285**, 1373 (1999).
 - ¹² C. C. Tsuei and J. R. Kirtley, Rev. Mod. Phys. **72**, 969 (2000).
 - ¹³ A. Sugimoto, T. Yamaguchi, and I. Iguchi, Physica C **367**, 28 (2002).
 - ¹⁴ V. G. Kogan, J. R. Clem, and J. R. Kirtley, Phys. Rev. B **61**, 9122 (2000).
 - ¹⁵ E. Goldobin, D. Koelle, and R. Kleiner, Phys. Rev. B **67**, 224515 (2003), cond-mat/0209214.
 - ¹⁶ A. Zenchuk and E. Goldobin, Phys. Rev. B **69**, 024515 (2004), nlin.ps/0304053.
 - ¹⁷ H. Susanto, S. A. van Gils, T. P. P. Visser, Ariando, H.-J. H. Smilde, and H. Hilgenkamp, Phys. Rev. B **68**, 104501 (2003).
 - ¹⁸ J. R. Kirtley, K. A. Moler, and D. J. Scalapino, Phys. Rev. B **56**, 886 (1997).
 - ¹⁹ E. Goldobin, N. Stefanakis, D. Koelle, and R. Kleiner, Phys. Rev. B **70**, 094520 (pages 7) (2004), cond-mat/0404091.
 - ²⁰ N. Lazarides, Phys. Rev. B **69**, 212501 (pages 4) (2004).
 - ²¹ N. Stefanakis, Phys. Rev. B **66**, 214524 (2002), nlin.ps/0205031.
 - ²² E. Goldobin, A. Sterck, T. Gaber, D. Koelle, and R. Kleiner, Phys. Rev. Lett. **92**, 057005 (2004).
 - ²³ E. Goldobin, H. Susanto, D. Koelle, R. Kleiner, and S. A. van Gils, Phys. Rev. B **71**, 104518 (pages 8) (2005), cond-mat/0410340.
 - ²⁴ H. Susanto, E. Goldobin, D. Koelle, R. Kleiner, and S. A. V. Gils (2004), cond-mat/0412295.
 - ²⁵ E. Goldobin, D. Koelle, and R. Kleiner, Phys. Rev. B **70**, 174519 (pages 9) (2004), cond-mat/0405078.
 - ²⁶ A. V. Ustinov, Appl. Phys. Lett. **80**, 3153 (2002).
 - ²⁷ B. A. Malomed and A. V. Ustinov, Phys. Rev. B **69**, 064502 (pages 8) (2004).
 - ²⁸ A. Kemp, A. Walraff, and A. Ustinov, Physica C **368**, 327 (2002).
 - ²⁹ V. K. Kaplunenko and A. V. Ustinov, Europ. Phys. J. B **38**, 3 (2004).
 - ³⁰ A. Buzdin and A. E. Koshelev, Phys. Rev. B **67**, 220504 (pages 4) (2003), cond-mat/0305142.
 - ³¹ E. Goldobin (2003), URL <http://www.geocities.com/SiliconValley/Heights/7318/StkJJ.htm>
 - ³² C. Nappi, M. P. Lissitski, and R. Cristiano, Phys. Rev. B **65**, 132516 (2002).
 - ³³ H.-J. H. Smilde, Ariando, D. H. A. Blank, G. J. Geritsma, H. Hilgenkamp, and H. Rogalla, Phys. Rev. Lett. **88**, 057004 (2002).
 - ³⁴ T. Kato and M. Imada, J. Phys. Soc. Jpn. **66**, 1445 (1997), cond-mat/9701147.
 - ³⁵ E. Goldobin, K. Vogel, O. Crasser, R. Walser, W. P. Schleich, D. Koelle, and R. Kleiner (2005), submitted, cond-mat/0504507.

³⁶ In this context "effective mass" actually means momentum of inertia $\sim 10^{-3} m_e \lambda_J^2$ (m_e is the electron mass and λ_J the Josephson penetration depth)³⁵

³⁷ Hypres, Elmsford, New York, USA.
<http://www.hypres.com>